minerals

MDPI

Article

Composition and Formation of Gabbro-Peridotite Hosted Seafloor Massive Sulfide Deposits from the Ashadze-1 Hydrothermal Field, Mid-Atlantic Ridge

Anna Firstova [1,2,*], Tamara Stepanova [1], Georgy Cherkashov [1,2,*], Alexey Goncharov [2] and Svetlana Babaeva [1]

[1] Institute for Geology and Mineral Resources of the Ocean (VNIIOkeangeologia), 1 Angliisky Ave., St. Petersburg 190121, Russia; steptv45@gmail.com (T.S.); babaevasvet@yandex.ru (S.B.)

[2] Institute of Earth Sciences, St. Petersburg State University, 7/9 Universitetskaya Emb., St. Petersburg 199034, Russia; a.goncharov@spbu.ru

* Correspondence: anetfirst@gmail.com (A.F.); gcherkashov@gmail.com; (G.C.); Tel.: +8-981-828-9973 (A.F.); +7-812–713-8378 (G.C.)

Academic Editor: Andrea Koschinsky-Fritsche
Received: 3 December 2015; Accepted: 22 February 2016; Published: 8 March 2016

Abstract: This paper presents mineralogical and geochemical data on seafloor massive sulfides (SMS) from the Ashadze-1 hydrothermal field at the Mid-Atlantic Ridge (MAR). The Ashadze-1 deposit is associated with the uplifted lower crust and upper mantle (oceanic core complex, OCC) of the MAR segment characterized by asymmetric mode of accretion. The OCC is represented by deep-seated gabbro-peridotite rocks exhumed on the rift valley slope along the detachment fault, during seafloor spreading. Hydrothermal processes in OCC environments result in different deposit composition and morphology compared to basalt-hosted systems. Abundant chimneys and enrichment in particular metals, including copper, zinc, gold, cobalt and tin are typical for this type of SMS deposit. The Ashadze-1 deposit is considered an example of a hydrothermal system in the initial stage of evolution marked by the young age of the sulfides (<7.2 kyr). The mineralogy of Ashadze-1 reflects primary ore-forming processes unaffected by post formation alteration. We propose a model for the primary ore-forming hydrothermal process in an ultramafic-hosted environment on the modern seafloor.

Keywords: seafloor massive sulfides; ultramafic hosted deposits; Mid-Atlantic Ridge; oceanic core complex; hydrothermal processes

1. Introduction

The first seafloor massive sulfide (SMS) samples from the Atlantic Ocean were recovered in 1985 [1]. Since 1985, more than 20 new hydrothermal fields with associated mineralization have been discovered on the Mid-Atlantic Ridge (MAR) [2,3]. Several of these systems have been discovered during Russian scientific and prospecting exploration activities in the Northern Equatorial MAR [4]. SMS deposits such as Ashadze, Irinovskoe, Semyenov, Logatchev (24°30′ N) and Pobeda (17°09′ N) (Figure 1) are associated with uplifted, lower crust and upper mantle, gabbros and peridotites. This rock package is known as an oceanic core complex (OCC). OCCs occur at MAR segments with an asymmetric mode of accretion [5]. OCC are tectonically uplifted along detachment faults, which exhume these deep-seated rocks onto the seafloor. OCC-associated SMS deposits are widely distributed at slow- and ultra-slow spreading ridges and are characterized by high grades of copper and gold [2,4].

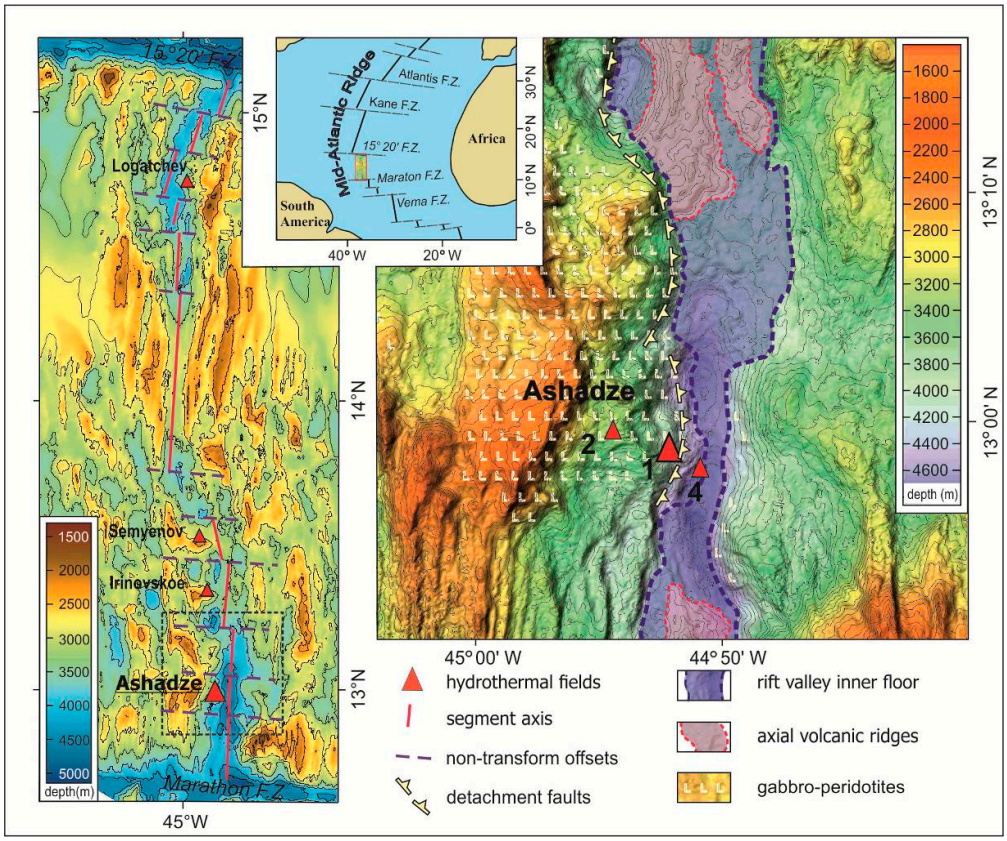

Figure 1. Ashadze hydrothermal field at the Mid-Atlantic Ridge bathymetry.

The Ashadze hydrothermal field is located at 12°58′ N, 15 miles to the north of the Marathon fracture zone (Figure 1). It was discovered in 2003 [6] and was revisited twice in 2005 and 2007 during cruises of Research Vessel Professor Logatchev. These investigations mapped two large separate hydrothermal deposits (Ashadze-1 at 4100 m and Ashadze-2 at 3300 m depth). The deposits are surrounded by metalliferous sediments on the western slope of the MAR (Figure 1) [7]. Ashadze-1 is located 1 km west of the inferred emergence zone of the detachment fault which separates gabbro-peridotites and volcanic basalts (Figure 1) [8]. Two ore bodies surrounded by the metalliferous sediments on the gabbro-peridotite basement compose the Ashadze-1 hydrothermal field (Figure 2).

In 2007, detailed studies of the Ashadze hydrothermal field were carried out using the Remotely Operated Vehicle (ROV) *Victor* and involved detailed near-bottom bathymetric and visual (photo and video) mapping as well as sampling of rocks and sulfides, during the French-Russian expedition "Serpentine" onboard Research Vessel Pourquoi Pas? [9]. High-resolution bathymetry (pixel size: 0.5–1 m) [8] and video profiling was used to describe the local geological setting and to get visual images of the Ashadze-1 deposit. Ondreas [8] and Cannat [10] proposed that the rockslides in the region, interpreted from the detailed bathymetric data, were associated with the Ashadze-1 hydrothermal field. The topography of the site is low, with elevation reaching 6 m above the seafloor. The deposit morphology is characterized by abundant sulfide chimneys observed from video profiling. Images from Ashadze-1 demonstrate unusual "forest-like" chimney accumulations (up to ten 30–40 cm high chimneys per one square meter) (Figure 3). This observation confirmed that massive sulfide samples collected during dredging operations from previous cruises are representative of hydrothermal chimneys and their fragments. The detection of high temperature hydrothermal activity confirmed present-day ore-forming processes at Ashadze-1 hydrothermal field.

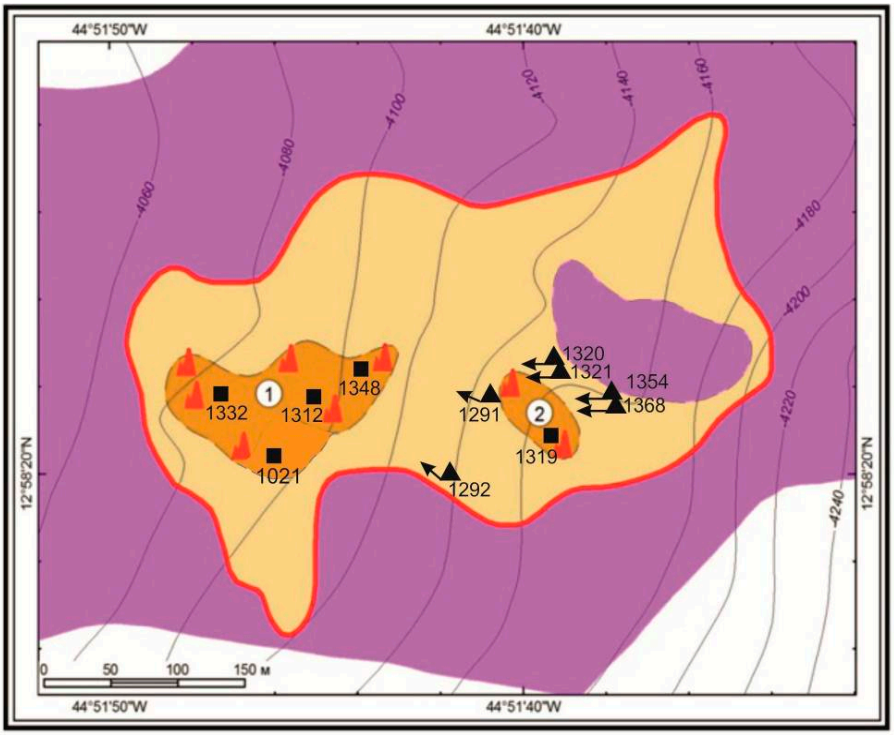

Figure 2. Gabbro-peridotite (violet) hosted Ashadze-1 hydrothermal field consists of two ore bodies (brown) surrounded by metalliferous sediments (yellow). Red figures—edifices detected by video profiling. Squares—grab samples with station number. Triangles—dredges with station number and direction of sampling on the seafloor.

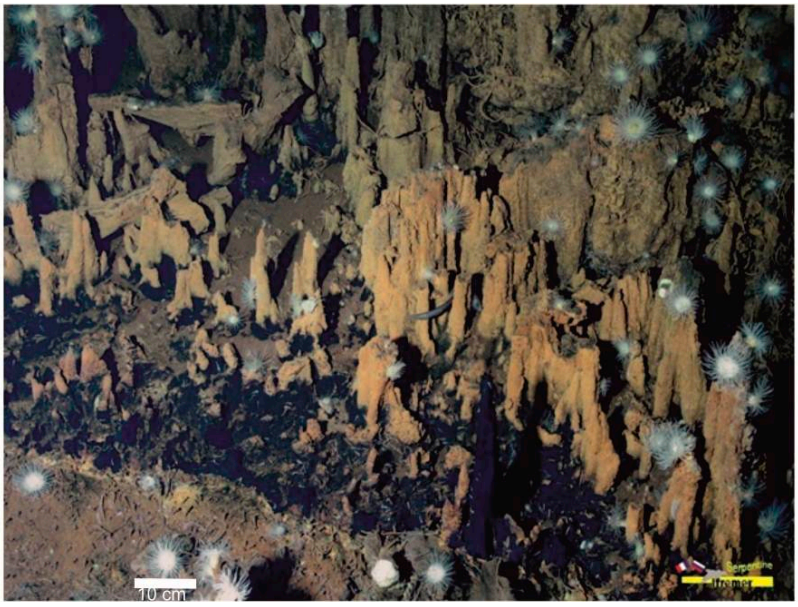

Figure 3. Image of chimneys accumulation ("forest-like") at the ore body 1 in the Ashadze-1 hydrothermal field. Chimneys are in different degree of oxidization. White actinias indicate present-day hydrothermal activity. Photo made by Remotely Operated Vehicle (ROV) *Victor* in French–Russian expedition Serpentine (2007), Copyright IFREMER (French Research Institute for Exploitation of the Sea).

We present data for sulfide mineralogy and geochemistry of samples from the Ashadze-1 SMS deposit collected during cruise 24 of RV Professor Logatchev (2005). We propose Ashadze-1 is an example of an OCC-associated SMS deposit in the primary stage of formation due to the young age of the sulfides (less than 7.2 kyr [4]) and the lack of significant hypergene alteration processes. The aim of this study is to propose a model for the initial evolution of ore-forming hydrothermal systems in ultramafic-hosted OCC environments on the modern seafloor.

2. Materials and Methods

In total, 55 sulfides samples have been studied. Initial description of mineralogy and structure of the samples was done on board. The major and minor mineralogical phases were identified using reflected light microscope and X-ray diffraction analyses (25 samples). X-ray diffraction analyses were done on D8 Advance Bruker AXS diffractometer (Cu Kα 35 kV 25 mA, French Research Institute for Exploitation of the Sea, Centre de Brest, Brest, France).

Whole rock chemistry (55 samples) was completed at the VNIIOkeangeologia (VNIIO), St. Petersburg: major oxides SiO_2 and Al_2O_3 were analyzed using a standard photometric method by Shimadzu uv-1650-pc spectrometer (VNIIO, St. Petersburg, Russia); major elements (Fe, Mn, Cu, Zn, Pb, Cd, Co, Ca, Mg) were determined using atomic absorption spectroscopy (C-155 spectrometer with flame atomization, VNIIO) with calibration by certified standards; trace elements Sr, As, Ni, Cr, Sc, Y, Sn, Bi, V, Ga, Ge, Ti, Zr, Tl, Ba, Ag were analyzed using quantitative optical emission spectroscopy on DPF-13 spectrograph (VNIIO) with plane grating in 600 line/mm, working range was 200–100 nm, relative aperture 1:40, linear dispersion of 0.4 nm/mm. Whole rock Au content was determined by chemical-spectral method.

Major element analyses of ore-forming minerals (31 samples) were done on a scanning electron microscope (SEM) Hitachi S3400N (Geomodel Center, St. Petersburg State University, St. Petersburg, Russia) with energy dispersive X-ray spectroscopy (EDX) detector AzTec Energy 350 (Geomodel Center, St. Petersburg State University) and wavelength dispersive X-ray spectroscopy (WDX) detector INCA 500 (Geomodel Center, St. Petersburg State University) (operators Vladimir Shylkovskyh and Natalia Vlasenko), using an acceleration potential of 20 kV, a beam current of 2 or 10 nA and a spot size from 3–5 μm for EDX and WDX procedures, respectively. Standards were natural minerals and pure oxides and metals. The presented results are based on 40 optical and 60 SEM images, as well as 350 point analyses of major and accessory minerals.

The $\delta^{34}S$ values (1σ = 0.3–0.4) of 17 samples and standard NBS—123 (sphalerite) were measured on a DELTA plus XL with preparative adapters (on line) EA 1112 and ConFlo III mass spectrometer at the Centre of Isotopic Research of VSEGEI, St. Petersburg, Russia.

3. Results

3.1. Mineralogical Types: Description and Characteristics

Recovered massive sulfides were represented by chimneys and their fragments. Based on the major mineral distribution, the chimneys are subdivided into chalcopyrite, pyrrhotite-isocubanite and sphalerite types. The mineral composition of the three chimney types is presented in Table 1 (based on X-ray, microprobe and optical analyses). A separate chapter will discuss the accessory mineralization.

Chalcopyrite chimneys were reported from half of the stations. The number of these types of samples varies from 75% of recovered material to just a few samples. Well-preserved chimneys are scarce and their fragments, 7–12 cm across and up to 30 cm long, are more typical (Figure 4a). The minor minerals are represented by isocubanite, bornite, roxbyite, digenite and geerite. Rare minerals are chalcocite, yarrowite and spionkopite (Table 1). Chemical compositions of chalcopyrite, isocubanite and bornite are presented in Table 2.

Table 1. Major and minor minerals of chimneys from Ashadze-1 field.

Sulfides	Chimney Type	Chalcopyrite					Pyrrhotite-Isocubanite					Sphalerite							
	Station / Mineral	1292	1368	1319	1354	1087	1319	1320	1321	1354	1368	1332	1319	1348	1321	1312	1291	1292	1021
Fe	Pyrite FeS_2						▫		Δ		Δ	▫	Δ				Δ		Δ
	Pyrrhotite $Fe_{1-x}S$							■	■	▫	▫				Δ	▫		▫	
	Marcasite FeS_2								▫	Δ					▫				
	Greigite $FeFe_2S_4$									Δ									
Zn	Sphalerite (Zn,Fe)S					▫	▫	■	▫	▫	▫	■	■	■	■	■	■	■	■
	Wurtzite (Zn,Fe)S											■	Δ	Δ					Δ
	Rudashevs Kyite-2H(Fe,Zn)S											▫							
Cu	Chalcopyrite $CuFeS_2$	■	■	■	■	■	■	▫	▫	■	▫	▫			▫		▫	Δ	▫
	Isocubanite $CuFe_2S_3$			▫	▫		■	■	■	■	■	▫			■	▫	▫	Δ	
	Y-phase $Cu_2Fe_3S_5$						Δ	Δ	Δ	Δ	Δ								
	Bornite Cu_5FeS_4		▫	▫	Δ	■													
	Chalcocite Cu_2S					Δ													
	Roxbyite Cu_9S_5			▫															
	Digenite Cu_9S_5					▫													
	Geerite $Cu_8\ S_5$					▫					Δ	Δ							
	Spionkopite $Cu_{1.4}S$	Δ									▫								
	Yarrowite Cu_9S_8	▫									Δ								
	Covellite CuS				Δ														
	Number of samples	1	1	1	1	1	1	2	1	4	1	2	1	1	2	1	1	1	3

Here ■ indicates dominant mineral >25%; ▫ indicates abundant mineral 25%–10%; and **Δ** indicates rare mineral <10%.

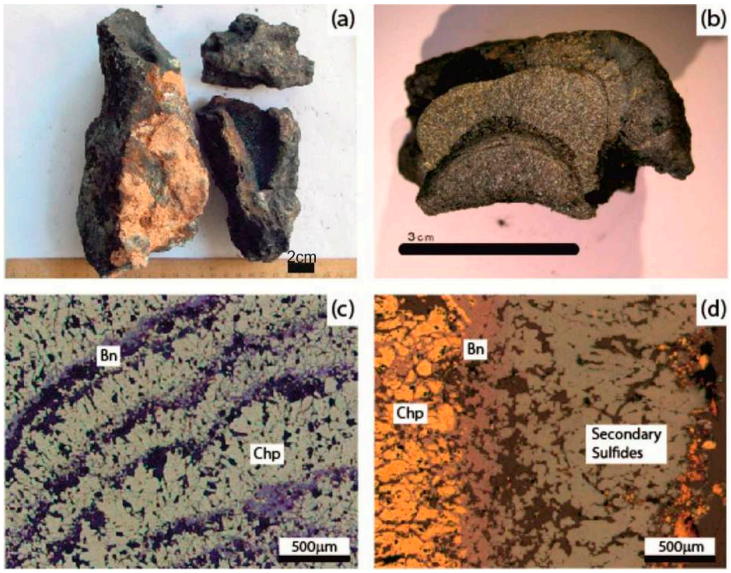

Figure 4. Chalcopyrite chimneys. (**a**) A general view of chalcopyrite chimneys with central conduit composed by lanciform chalcopyrite. The outer zone is composed of secondary sulfides; (**b**) Layered structure of chimney with secondary Cu-sulfide in the outer zone and rhythms separated by a smooth and polished surface; (**c**) A granular and lanciform chalcopyrite forming rhythmic-layered texture. Bornite occurs at the rhythms contacts (polished-section); (**d**) The outer oxidized zone is composed of secondary Cu-sulfides at the contact with chalcopyrite. The contact is represented by bornite.

Table 2. Chemical composition of chalcopyrite chimneys minerals.

Mineral (Number of Analyses)	Element (wt %)					
	Fe	**Cu**	**Zn**	**Co**	**Ni**	**S**
	Average Min.–Max.	**Average** Min.–Max.	**Average** Min.–Max.	-	**Average** Min.–Max.	**Average** Min.–Max.
Chalcopyrite (8)	**31.85** 31.35–32.15	**33.92** 31.35–32.15	**0.17** 0–1.12	-	-	**34.04** 33.5–34.96
Isocubanite (3)	**41.2** 39.56–43.52	**23.92** 21.16–25.86	**0.15** 0–0.37	-	**0.003** 0–0.01	**34.68** 34.55–34.95
Bornite (6)	**13.91** 11.51–19.21	**60.93** 55.09–63.91	**0.002** -	-	-	**25.15** 24.11–26.55

Two mineralogical zones are recognized in the chalcopyrite chimneys (Figure 4b). Generally, an inner chalcopyrite zone and an outer secondary bornite and Cu-sulfide zone surround a single conduit (Figure 4b,c). The inner chalcopyrite zone consists of rhythmic, dual textured layers, where each layer is defined as a rhythm (Figure 4c). In some places up to twelve rhythms have been identified in the chimney. Each rhythm consists of two textural zones (Figure 4b). An inner zone of radial-fibrous aggregates of flattened (lanciform) chalcopyrite (up to 5 mm thick) with isocubanite occurring in the central parts of the chalcopyrite crystals, grading outwards into a dense, microgranual chalcopyrite zone (up to 2 cm thick). This outer microgranual zone forms a smooth, almost polished, surface along which the chimney easy breaks. Bornite occasionally occurs at the contact between each rhythm (Figure 4c). The outer mineralogical zone consists of bornite and non-stoichiometric Cu-sulfides (1.5 to 3 cm thick) of the geerite-covellite series, such as yarrowite and spionkopite (Table 1, Figure 4d). At the contact of two mineralogical zones, chalcopyrite is dissected by a series of zonal veinlets whose central part is composed of Cu-sulfides and a bornite rim.

Pyrrhotite-isocubanite chimneys were found in varying abundance at the same stations as those with chalcopyrite ones. They are represented as both large fragments (12–15 cm across, 30–35 cm long) and smaller coalescent chimneys. The pyrrhotite-isocubanite type differs from the chalcopyrite type in that the chimneys are massive and have no central conduit (Figure 5a). The minor minerals are represented by sphalerite, chalcopyrite and pyrite-marcasite replacing pyrrhotite, and a rare typomorphic Y-phase mineral (Table 1). The chimneys are massive, porous, granular pyrrhotite-isocubanite aggregates penetrated by conduits of different size and orientation (Figure 5b). A thin sphalerite layer occurs sporadically in the outer part (Figure 5c). Chimneys of this type are marked by subsequent transformation of major minerals. Tabular pyrrhotite exhibits a varying degree of alteration: ranging from the replacement of rims by greigite and thin-grained Fe-sulfides to a boxy pyrite-marcasite pseudomorph (Figure 5d) Xenomorphic isocubanite without a decomposed texture has brown-yellow color and shagreen surface. Microprobe analyses made it possible to assign these formations to the Y-phase (Table 3, Figure 5e), an intermediate between chalcopyrite and isocubanite [11].

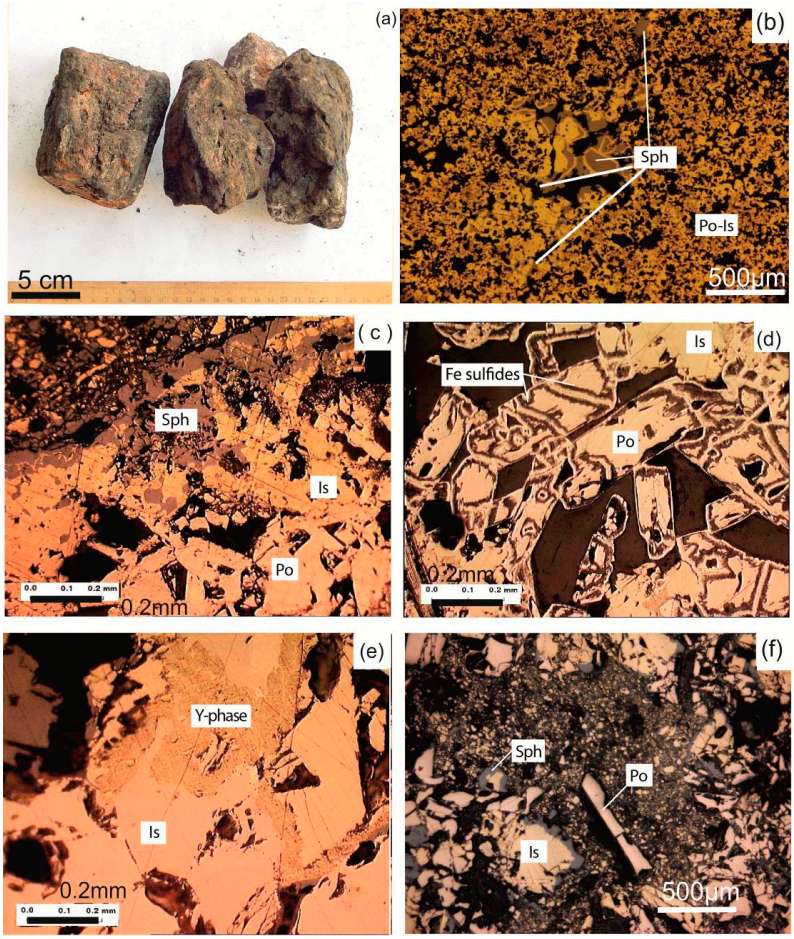

Figure 5. Pyrrhotite-isocubanite chimneys. (**a**) A general view of pyrrhotite-isocubanite chimneys. The chimneys are massive and porous. Pyrrhotite-isocubanite aggregates are penetrated by conduits of different size and orientation, a thin sphalerite layer occurs sporadically in the outer part; (**b**) Sphalerite (II generation) in cracks and vesicles of pyrrhotite-isocubanite aggregates (I generation). Pyrrhotite-isocubanite assemblages in the central part of chimney; (**c**) The inner pyrrhotite-isocubanite and the outer sphalerite zones contact. Clastic aggregate occurs at the contact (**d**) Pyrrhotite plates are partly replaced by Fe-sulfides. Sample 1354-T-3; (**e**) Isocubanite alternation: isocubanite transforms into Y-phase with darker color and shagreen surface; (**f**) Fine-fragmented aggregates in pyrrhotite-isocubanite chimneys mark areas of dissolved anhydrite

Table 3. Chemical composition of pyrrhotite-isocubanite chimneys minerals.

Mineral (Number of Analyses)	Element (wt %)					
	Fe	**Cu**	**Zn**	**Co**	**Ni**	**S**
	Average Min.–Max.	**Average** Min.–Max.	**Average** Min.–Max.	**Average** Min.–Max.	**Average** Min.–Max.	**Average** Min.–Max.
Pyrrhotite (8)	**61.83** 61.35–62.15	-	-	**0.42** 0.14–0.65	**0.04** 0–0.13	**37.7** 37.24–38
Pyrite-marcasite (5)	**42.77** 33.04–48.48	**0.11** 0–0.37	**0.8** 0–2.41	**1.14** 0.47–1.96	**0.15** 0–0.24	**55.07** 49.52–63.35
Chalcopyrite (7)	**31.68** 27.76–35.41	**32.15** 29.66–34.06	**1.63** 0–4.75	**0.3** 0–0.64	-	**34.22** 30.57–34.78
Isocubanite (12)	**42.74** 40.54–43.91	**22.09** 20.89–24.46	**0.23** 0–0.82	**0.38** 0–0.75	**0.01** 0–0.19	**34.49** 33.17–35.18
Y-phase (4)	**37.67** 36.53–39.21	**26.79** 25.14–28.48	**0.32** 0.09–0.7	**0.08** 0–0.31	-	**35.12** 33.93–37.66
Sphalerite (6)	**15.06** 5.82–21.67	**0.37** 0–0.76	**51.26** 46.15–60.8	**0.24** 0.02–0.41	**0.07** 0–0.2	**33.0** 31.9–33.61

Sphalerite has corroded relict in the isocubanite grains. Sphalerite occurs in cracks and vesicles of pyrrhotite-isocubanite aggregates (I generation) (Figure 5b). In superimposed conduits, pyrrhotite, isocubanite and sphalerite form druses of unaltered, relatively coarse-grained subidiomorphic crystals. Obscured ring structures emphasized by a cavity arrangement occur at the contact with the sphalerite layer. The sphalerite layer contact is sharp, with clastic aggregates occurring at the contact (Figure 5e). A fine-fragmented texture occurs locally in the central part of the chimney (Figure 5f). The outer layer is composed of dendrite or granular sphalerite. Fe-content in sphalerite varies and averages 15.06 wt % (Table 3).

Sphalerite chimneys are represented by single fragments with up to 85% sulfides and occur at most stations. Coalescent small chimneys up to 10 cm across are common (Figure 6a). Chimneys up to 50 cm in diameter were observed protruding from sediments. The minor minerals are represented by pyrrhotite, wurtzite, isocubanite, chalcopyrite and pyrite (Table 1).

Most chimneys exhibit a clear zonal structure with two layers of variable thickness: a central massive porous layer with sphalerite-pyrrhotite-chalcopyrite-isocubanite (Figure 6b) and an outer layer represented by sphalerite (Figure 6c). Large chimneys and their aggregates have a sphalerite layer with colloform-porous Fe-sulfides containing a local admixture of mineralized hydrothermal biogenic fossils. Small chimneys (up to 10 cm in diameter) have a hollow central conduit. Conversely, large chimneys (up to 50 cm in diameter) consist of a system of small convergent conduits.

The central massive-porous layer consists of sphalerite-isocubanite-pyrrhotite aggregate. Isocubanite is graduated and granular. Exsolution texture of decomposed isocubanite was observed. The largest lamellas reach 5–10 μm in width and 30–40 μm in length. The second order exsolution textures occur when the matrix between large lamella is dissected by a net of smaller lamella. Isocubanite grains have a chalcopyrite rim. Pyrrhotite occurs as small plates in the aggregates. Pyrrhotite crystals reach 2 mm in large cavities and in the conduits (Figure 6b). Fine sphalerite crystals overgrow isocubanite and pyrrhotite.

The outer black-brown sphalerite layer has mainly dendritic structure with powder-like or granular parts. Sphalerite has a nodular, colloform texture and forms as dendritic, rhythmic layered intergrowth with isocubanite and chalcopyrite (Figure 6c). Fine sphalerite crystals in pores reach 0.2 mm. Isocubanite, chalcopyrite and pyrrhotite occur as small patches (spots) or bands. Sphalerite in the shalerite-type chimneys contains half the amount of Fe compared to the pyrrhotite-isocubanite chimneys (Table 4). Fe content does not exceed 5 wt % in sphalerite low-temperature chimneys.

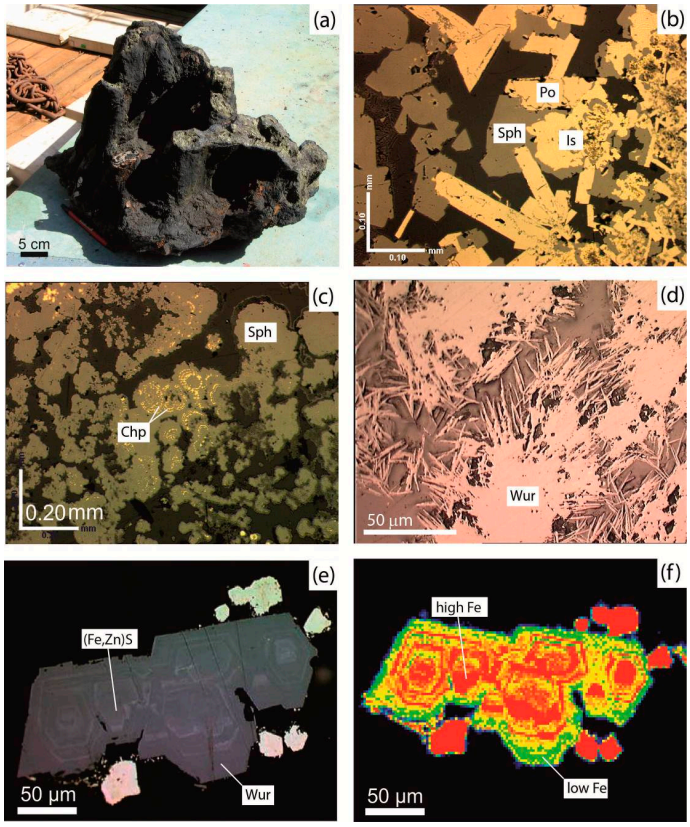

Figure 6. Sphalerite chimneys. (**a**) A general view of coalescent sphalerite chimneys. Station 1320. (**b**) Central part of sphalerite chimney is constructed of pyrrhotite and isocubanite. Unaltered pyrrhotite plates with isocubanite are overgrown by sphalerite. Sample 1312-T-2; (**c**) The outer zone of chimney is composed of nodular, colloformic sphalerite. Chalcopyrite occurs as rhythmic zones in sphalerite. Sample 1312-T-1; (**d**) Wurtzite plates in high-temperature sphalerite chimneys; (**e**) Rudashevskyite zone in wurtzite crystals; (**f**) Fe distribution in wurtzite crystals marked rudashevskyite.

Table 4. Chemical composition of sphalerite chimneys minerals.

Mineral (Number of Analyses)	Element (wt %)					
	Fe	Cu	Zn	Co	Ni	S
	Average Min.–Max.	**Average** Min.–Max.	**Average** Min.–Max.	**Average** Min.–Max.	**Average** Min.–Max.	**Average** Min.–Max.
Pyrrhotite (5)	**60.07** 58.16–62.24	**0.04** 0–0.18	**0.24** 0–1.19	-	-	**39.65** 36.49–41.86
Pyrite (2)	**35.91** 35.52–36.3	**1.35** 0.99–1.71	**12.79** 11.84–13.74	-	-	**49.95** 48.98–50.93
Chalcopyrite (2)	**27.95** 27.21–28.69	**30.52** 28.81–32.23	**6.41** 3.01–9.81	-	-	**35.07** 34.17–35.98
Isocubanite (4)	**42.87** 40.29–44.26	**21.41** 20.51–22.56	**1.07** 0–2.73	**0.05** 0–0.2	**0.02** 0.08	**34.57** 33.9–35.24
Sphalerite (30)	**7.7** 1.16–20.17	**1.27** 0.–4.34	**57.87** 42.46–65.36	-	**0.01** 0–0.12	**33.11** 31.86–34.41

There are a number of samples composed mainly of Zn-sulfides and with a thick central layer (up to 0.5 mm width). These small chimneys (up to 10 cm) and edifices grow directly on ultramafic

rock and form platy flanks on the chimneys. All of them are characterized by platy, high Fe-wurtzite (Figure 6d) or compositionally zoned Zn-sulfides. Wurtzite with Fe-content amounting 50 wt %, enables us to consider this mineral as a Fe-wurtzite polytype which can be named rudashevskyite-2H by analogy with Fe-sphalerite polytype (Figure 6e,f).

3.2. Geochemical Characteristics

Ashadze-1 deposits as a whole as compared to sulfides of MAR are strongly enriched in Co (average = 2373 ppm) and Ni (average = 250 ppm), as well as Cu (average = 12.14 wt %), Zn (average = 21.51 wt %) and zinc-associated elements: Cd (average = 329 ppm), Pb (average = 319 ppm), Ag (average = 99 ppm) and especially Sn (average= 419 ppm) (Table 5).

Table 5. Average element concentrations in SMS.

Elements		Sulfides					
		Type of Chimneys				MAR * (Our Data)	Basalt-Hosted [12]
		Chalcopyrite	Pyrrhotite-Isocubanite	Sphalerite	All Types of Chimneys (Our Data)		
Fe	wt %	27.51	35.20	21.81	25.73	32.43	30.75
S		29.52	31.55	25.86	27.86	36.44	34.06
Cu		**31.00**	**15.02**	5.06	12.14	9.56	9.64
Zn		0.33	**7.57**	**33.41**	**21.51**	4.39	5.21
Si		0.31	0.50	0.52	0.48	3.2	12.1
Ca		0.80	0.23	0.61	0.53	0.42	1.51
Mg		0.14	0.17	0.19	0.17	0.14	0.4
Al		0.23	0.08	0.16	0.14	0.16	0.25
Ti	ppm	300	697	381	468	450	220
Co		**3200**	**5362**	**941**	**2373**	619	200
Ni		***1262***	16.5	5.9	**250**	55.4	29
Bi		2.1	**5.7**	2.6	3.5	4.5	2.2
Se		**1237**	33	12	229	280	11
Pb		5.0	73.5	**523**	**319**	157	33
Ga		4.9	10.2	12.2	10.2	19.1	41,2
Ge		2.0	15.5	**78.7**	43,9	36.1	39.2
Sn		32.6	**164.2**	***713***	**419**	64.5	20.9
Cd		4.3	126.2	**516**	**329**	110	190
Sb		25.0	25.0	**70.6**	**50.6**	32.9	n.d.
As		57.1	94.6	186	130	318	270
Mn		23.9	39.1	**271**	158	159	483
Ba		105.0	126.9	**1171**	664	2900	790
Ag		0.5	23.5	**155**	**99.7**	3.2	77.2
Au		1.9	**6.4**	1.9	2.9	48.5	3
n		10	15	30	55	1051 *	427
Age, kyr [4]		6.2 ± 1.5	7.2 ± 1.8	7.1 ± 0.6; 5 ± 0.9; 3.3 ± 0.3; 2.1 ± 0.3	-	-	-

Note: ***italic***—>10 times higher than average on Mid-Atlantic Ridge (MAR) sulfides; **underlined**—5–10 times higher than average on MAR sulfides; **bold**—1.5–5 times higher than average on MAR sulfides; n.d.—not determined. * massive sulfides data (Fe + Cu + Zn > 25%, *n* = 1051).

Chalcopyrite chimneys have Cu enrichment and are characterized by high concentrations of Cu (average = 31 wt %), Co (average = 3200 ppm), Ni (average = 1262 ppm) and Se (average = 1257 ppm). A relative depletion in Zn and its associated elements (especially Ag—0.5 ppm) as well as low Au content (1.92 ppm) are also characteristic features of these types of chimneys.

Pyrrhotite-isocubanite chimneys have Cu-Zn enrichment. Cu content (average = 15 wt %) is twice as large as Zn (average = 7.6 wt %). As compared to other ore fields (Table 5), these

chimneys are extremely enriched in Co (average = 5362 ppm), Bi (average = 5.7 ppm) and Au (average = 6.4 ppm). They differ greatly from chalcopyrite chimneys in low Ni (average = 16.5 ppm) and Se (average = 33 ppm) contents.

Sphalerite chimneys have Zn-Cu enrichment dominated by Zn (average = 33.41 wt %) over Cu (average = 5.1 wt %) and strong enrichment of Zn associated elements: Cd, Ag, Pb, Sb, Ge and Sn (Table 5). Chimneys with high ferric Zn-sulfides exhibit high Zn concentrations (average = 53–63 wt %) from outgrowth and edifices which are growing directly on the gabbro-peridotite basement. These samples also have maximal concentrations of Sn (1100–1800 ppm), Ge (110–200 ppm) and Cd (600–1100 ppm). Au content in sphalerite chimneys is insignificant (average = 1.95 ppm). Unlike other chimneys, they contain high Mn and Ba concentrations.

3.3. Accessory Mineralization

Using microprobe analyses, numerous accessory minerals of rare elements were identified in all three types of chimneys (Table 6). We note that rare elements occur in their mineral forms (for example, Co in cobaltite (Table 6)) but also replace other elements in other mineral crystal lattices (for example, Co in chalcopyrite or pyrrhotite (Table 3).

Chalcopyrite chimneys have high cobalt and nickel contents. These elements were found in minerals such as cobalt-pentlandite and millerite, which could be considered as the main typomorphic minerals of chalcopyrite chimneys. Co-pentlandite, discernable even on optical investigation, occurs at the bornite-chalcopyrite contacts (Figure 7a). Millerite is not common and often occurs in granular or massive chalcopyrite. Nickel telluride—melonite (with Bi content up to 1.2 wt %) was recorded in a single sample in chalcopyrite (Figure 7b). Despite a low Au concentration, native gold was reported in isocubanite-chalcopyrite aggregates.

Pyrrhotite-isocubanite chimneys are marked by enrichment in cobalt, bismuth and gold. High Co concentration was confirmed by the presence of Co-minerals and was detected in major minerals (Table 3). Co-mineralization in this type of chimney differs from that of chalcopyrite chimneys. Co-As minerals (cobaltite, glaucodite, *etc.*) are common (Figure 8a). These minerals occur at the contact of sphalerite-pyrrhotite-isocubanite aggregates in cracks and intergranular space. Sphalerite in this aggregate is characterized by high Fe content (up to 21.26 wt %) (Figure 8b). Au, which is associated with altered isocubanite-chalcopyrite aggregates, occurs in native form (Figure 8c). Another variety of Au, electrum, is associated with unaltered sphalerite-chalcopyrite and sphalerite-isocubanite aggregates. It occurs in cracks and pores. Rare stibnite (SbS) grains were reported from isocubanite aggregate. Sb was also commonly detected in cobaltite and sphalerite. The great variety of Co-As minerals associated with Fe-sphalerite in intergrowth with unaltered pyrrhotite and isocubanite is a specific feature of this type of chimney.

Sphalerite chimneys are characterized by high Sn, Cd, Ge, Pb and Ag concentrations. Fe content in sphalerite varies from 1.16–20.17 wt %. Cd was detected in sphalerite. The presence of Sn (up to 5 wt %) in sphalerite with high Fe content or in Zn-sulfides was a feature of this type of chimney (Figure 9a). Electrum and cobaltite are also associated with Zn-sulfides with high Fe content. Minerals of Pb and Ag are associated with dendritic sphalerite with low Fe content (Table 4, Figure 9b–d). Galena is the typomorphic mineral of sphalerite chimneys and often related to low-temperature sphalerite.

Typomorphic minerals of rare elements in sulfides chimneys from Ashadze-1 are minerals of Co, Ni and Au, rarely Ag; Pb Minerals such as cobaltite, glaucodite, skutterudite and carrolite were found for the first time in Ashadze-1 chimneys (Table 6).

Depending on relationships between grades and presence of mineral phase rare elements, they are subdivided into three groups:

(1) Co, Ni, Sb, Pb and Ag form minerals with high concentrations of these elements.
(2) Au forms in minerals despite its low concentrations.
(3) Sn, Cd, Se and Ge are detected in major and minor minerals, interpreted as having replaced other elements in the crystal lattice of the analyzed mineral and do not form minerals.

Table 6. Minerals of rare elements occurrence in different type of chimneys.

Chimney Type	Chalcopyrite					Pyrrhotite-Isocubanite					Sphalerite							
Station / Mineral	1292	1368	1319	1354	1087	1319	1320	1321	1354	1368	1332	1319	1348	1321	1312	1291	1292	1021
Co-pentladite $(Co,Fe,Ni)_9S_8$	+	+	+	+	+													
Millerite NiS	+	+									+							
Cobaltite CoAsS						+	+	+	+		+	+		+	+		+	+
Glaucodite (Co,Fe)AsS							+		+	+		+			+			+
Carrollite $CuCo_2S_4$						+		+	+	+								
Skutterudite $(Co,Ni)As_3(CoAs_3)$							+			+								
Melonite $NiTe_2$		+																
Native gold Au	+	+			+		+											
Electrum AuAg						+	+	+	+	+		+	+	+				
Native silver Ag											+		+	+		+	+	+
Acanthine Ag_2S																		+
Ag-pyrite $AgFe_2S_3$																		+
Stibnite Sb_2S_3								+		+								
Galena PbS							+	+	+		+	+	+	+	+	+	+	+
Boulangerite $Pb_5Sb_4S_{11}$								+										
Number of samples	1	1	2	2	1	2	4	1	4	1	1	2	1	2	2	1	2	1

Note: +—the mineral presence.

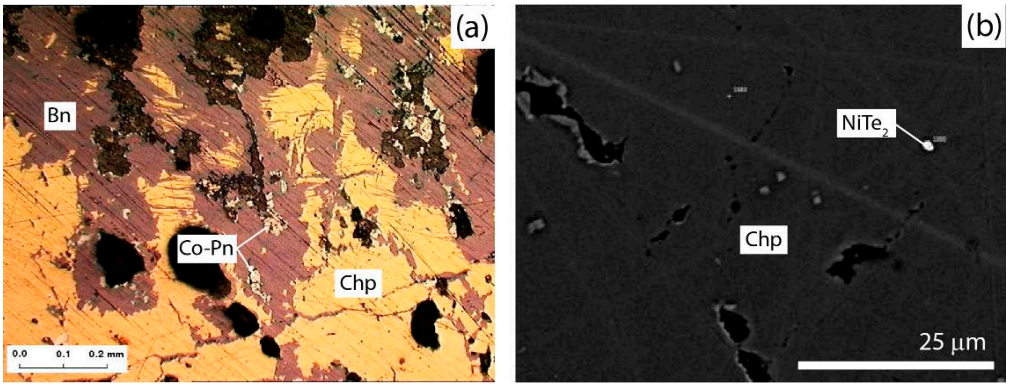

Figure 7. Minerals of rare elements in chalcopyrite chimneys. (**a**) Co-pentlandite at the chalcopyrite and secondary Cu-sulfides contact. (**b**) Melonite grain in granular chalcopyrite.

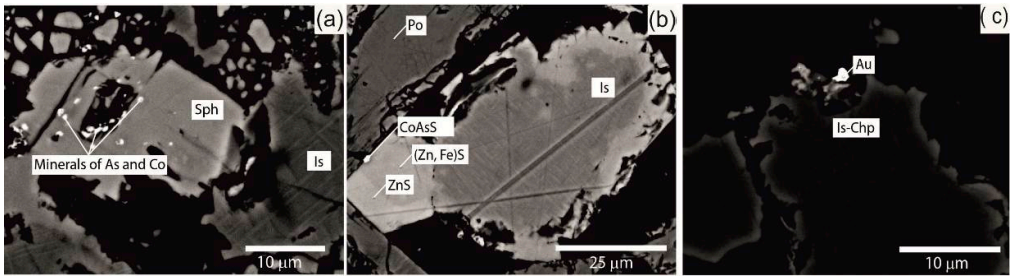

Figure 8. Minerals of rare elements in pyrrhotite-isocubanite chimneys. (**a**) Minerals of Co and As in sphalerite-isocubanite aggregates; (**b**) Cobaltite is associated with Fe-sphalerite grain; (**c**) Native gold in pore of isocubanite-chalcopyrite aggregate.

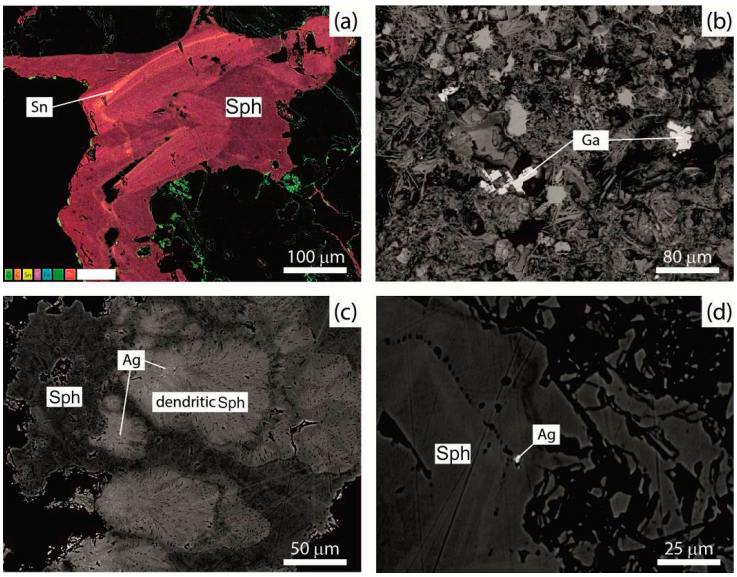

Figure 9. Rare elements in sphalerite chimneys. (**a**) The Sn distribution in sphalerite. (**b**) Galena grains; (**c**) Ag-mineralization in low-temperature dendritic sphalerite; (**d**) Native silver in zonal sphalerite.

Generally, regarding accessory mineralization, Ashadze-1 deposit is characterized by wide diversity of Co-minerals which are typical for ultramafic-hosted sulfides. Co in high-temperature

chalcopyrite chimneys occurs in Co-pentlandite. However, Co occurs in Co-As minerals as well as being detected in sphalerite in pyrrhotite-isocubanite chimneys, which indicates lower temperature parameters. Au associated with high-temperature chalcopyrite-isocubanite aggregates occurs in native form and occurs as electrum when associated with lower-temperature sphalerite.

Thus, accessory mineralization is related to specific mineral types with particular parameters of ore-forming processes.

3.4. Isotopic Studies of Sulfur

Sulfur isotopic composition was studied in chalcopyrite (isocubanite), sphalerite and pyrrhotite. In general, $\delta^{34}S$ values vary from +3.7‰–+14.1‰, averaging +5.8‰(Table 7).

Table 7. Sulfur isotopic composition in major minerals.

Type of Chimney	Sample	$\delta^{34}S$ (‰)			
		Chalcopyrite	Isocubanite	Sphalerite	Pyrrhotite
Chalcopyrite	1319-T-10	+4.3			
	1319-T-10 (I)	+3.7			
	1319-T-10 (II)	+3.7			
	1354-T-1/1	+3.9			
	1368-T-1	+4.5			
Pyrrhotite-Isocubanite	1319-T-2		+4.5		
	1319-T-2/1		+3.8		
	1354-T-3		+4.4		
	1354-T-3/2		+6.5		
	1354-T-3/3		+7.3		
	1354-T-4		+7.1		
Sphalerite	1354-T-5/1			+4.1	
	1321-TK-2/1			+4.4	
	1321-TK-1				+4.4
	1319-T-3/2			+6.4	
	1312-T-2		+7.8		
	1021-T-1			+11.9	+14.1

The isotopically lightest and slightly variable $\delta^{34}S$ is identified mainly in chalcopyrite chimneys and varies from +3.7‰–+4.5‰ (average +4.1‰). These values correspond to the isotopic characteristics of minerals formed directly from the initial portions of the fluid.

In pyrrhotite-isocubanite chimneys the $\delta^{34}S$ has wider range: from +3.8‰–+7.3‰ (average +5.6‰). There are two groups of values: minerals formed from the initial portions of fluid correspond to $\delta^{34}S$ +3.8‰–+4.5‰ and heavier sulfur isotope +6.5‰–+7.3‰.

The widest scatter of sulfur isotopic composition identified in sphalerite and pyrrhotite of sphalerite chimneys was +4.1‰–+11.9‰ and +4.4‰–+14‰, respectively.

Chapter 4.2 will discuss the reasons of wide varieties sulfur isotopic composition.

4. Discussion

4.1. Source of Metals and Ore-Forming Factors

Geochemical and mineralogical data demonstrates significant difference between ultramafic-hosted SMS from Ashadze-1 and the MAR deposits associated with basalts (Table 5). The most prominent feature is the high Cu + Zn content (~30 wt %). Such enrichment cannot be explained by gabbro-peridotites as source rocks because the concentrations of these elements are higher in basalts [2]. However, serpentinites of Rainbow field characterized by high values of Cu and Zn [2] could be considered as another source of metals for ultramafic sulfides.

A key observation is the lack of pyrite in the Cu-Zn-enriched chimneys at Ashadze-1. The only observed pyrite formed a thin, inconsistent layer on some of the chimneys and partly replaced pyrrohotite. This important feature is in contrast with basalt-hosted sulfides that exhibit pyrite abundance [13]. The lack of pyrite is critical in the interpretation that the ultramafic-hosted Ashadze-1 is in an initial stage of ore formation. Pyrite is observed in other ultramafic deposits, for example, Irinovskoe, however, these systems are more mature. Pyrite may precipitate during later stages of development of the hydrothermal system.

Pyrrhotite rather than pyrite is deposited from high-temperature reduced fluids. However, the formation of iron monosulfide or disulfide depends on the concentration of H_2S^- in the fluid, rather than temperature [14]. Iron is deposited from the hydrothermal fluid in the pyrite or pyrrhotite phase with higher or lower sulfur concentration, respectively. H_2S content varies from 0.1–1.9 mM (average 1.1 mM) and from 2.5–11 mM (average 6.3 mM) in hydrothermal fluids from ultramafic- and basalt-hosted fields, respectively [15]. As a result, pyrrhotite is preferentially deposited in a low H_2S environment. Therefore, the absence of pyrite is likely associated with deficiency of reduced sulfur, which may be deposited in the stockwork zone below in pyrrhotite.

The above statement is confirmed by the sequence of the minerals formation based on the thermodynamic modeling result (Figure 10) [16,17]. Pyrrhotite is the first to precipitate followed by the formation of sphalerite and chalcopyrite. These sulfides are deposited concurrently from end-member fluid at a temperature of 330–250 °C. In comparison, the deposition of pyrite starts at a temperature of about 50 °C from a fluid mixed with seawater. The obtained experimental data correlates well with observations and corroborates our explanation for some features of chimney composition, such as deposition of chalcopyrite and sphalerite coupled with extremely low pyrite content.

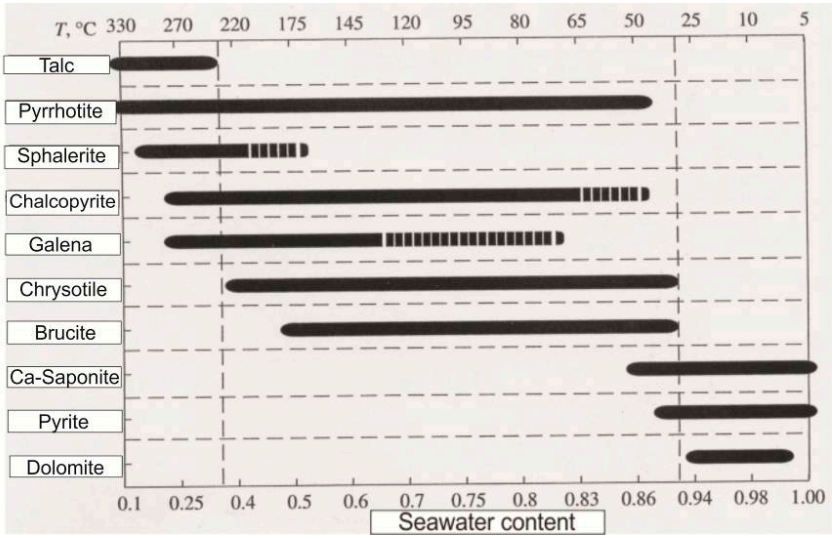

Figure 10. The sequence of the minerals formation of a high-temperature chimney related to ultramafic rocks (result of thermodynamic modeling) [16,17]. Reproduced with permission from Silant'ev, S.A., (*Petrology*); published by (International Academic Publishing Company (IAPC) "Nauka/Interperiodica 2009").

Ashadze-1 deposit is also enriched in Co and Ni. High Co values are concomitant with increased Cu sulfide content of the chimney. Nickel (and Se) enrichment was reported only from high-temperature chimneys (Table 5).

Gold is the typomorphic element of sulfides related to ultramafic rocks [2]. Our observations indicate at early high-temperature stages of hydrothermal system evolution gold does not reach significant values. The average Au content is 2.9 ppm, which is similar to Au concentration in sulfides

related to basalts (3 ppm). The mineral phases of Au, such as native gold and electrum, have been detected in sulfide chimneys in spite of relatively low concentrations.

4.2. Sulfur Isotope

The sulfide samples exhibit a wide range of $\delta^{34}S$ values, ranging from +3.7‰–+14.1‰. Previous models have attempted to explain the range of $\delta^{34}S$ [18–24]. Here we assess and attempt to apply the most appropriate model to explain the heavy sulfur isotope enrichment of sulfide minerals at Ashadze-1.

Chalcopyrite from the chalcopyrite rich chimneys exhibit $\delta^{34}S$ values of ~+4‰ (Table 7). These values are higher than those of sulfides from basalts formed through reaction of heated seawater; this process records $\delta^{34}S$ values of between +2.3‰–+4‰ [18]. Instead, the range of $\delta^{34}S$ results from reduction of seawater sulfate, through reaction with Fe^{2+} in the basement rock and conversion of pyrrhotite to pyrite during the seawater circulation (hydrothermal) process [19]. Generally, $\delta^{34}S$ values for fluids in ultramafic systems reach 2‰–3‰, for example, in Rainbow and Logatchev [20], whereas values in basalt-hosted systems fluctuate around 1‰. Bogdanov *et al.* [20] note that sulfate reduction plays a more critical role in ultramafic systems, due to sulfide disseminations in these rocks containing more isotopically-heavy sulfur than those in basaltic systems [21]. Based on this interpretation, we suggest that $\delta^{34}S$ values from chalcopyrite in chalcopyrite-rich chimneys reflect sulfur isotopic composition of the initial portions fluid of the young hydrothermal system. The increased values to 4‰ might be associated with stronger flooding of serpentinites and abundant sulfide disseminations in peridotite of the Ashadze-1 field.

Isocubanite from pyrrhotite-isocubanite chimneys exhibits different values of $\delta^{34}S$. The $\delta^{34}S$ of isocubanite has two ranges: +3.8‰ to +4.5‰ and +6.5‰ to +7.3‰. Minerals of the first group probably precipitate in a similar way to the chalcopyrite type chimneys, as mentioned previously, from the initial portion of the fluid. A further increase in the heavy isotope sulfur content is likely associated with dissolution reactions, substitution (replacement) and re-deposition on shallow horizons around chimneys and in the chimneys. Shanks and Seyfried [22] and Woodryff and Shanks [23] explain this process by the inclusion of seawater sulfate (anhydrate and pore water) with more heavy isotopic composition in precipitated sulfides. They also proposed a mechanism for recovery of sulfate by Fe^{2+}. We suggest that isocubanite enriched in isotopically-heavy sulfur formed during anhydrate replacement. Fine-clasted areas of dissolved anhydrate might be indirect evidence of the presence of anhydrate in the chimneys wall (Figure 5f).

There are three groups of $\delta^{34}S$ values in the sulfides of the sphalerite-type chimneys. Values ranging between $\delta^{34}S$ +4.1‰–+4.4‰ correspond to initial portions of fluid. $\delta^{34}S$ values of +6.4‰–+7.8‰ occur during replacement and re-deposition reactions. The highest values (+11‰–+14‰) of heavy sulfur are likely related to the process of reduction of seawater sulfate in shallow, subsurface mixing [24]. In this process, an additional amount of sulfate is recovered in the reaction of Fe^{2+} in the chimneys walls, or in the subsurface zone. The high and fluctuating values of $\delta^{34}S$ are produced in this process [24]. Values in sample 1021 (related to low-temperature type) (Table 7) indicate bacterial sulfate reduction is involved in production of a significant amount of heavy sulfur.

Our isotopic sulfur composition data confirms features of hydrothermal systems related to serpentinized peridotites, such as fluid enrichment in isotopically heavy S and the wide scatter of $\delta^{34}S$ in sulfides (e.g., Bogdanov [20]).

4.3. Formation

1. ***Chalcopyrite chimneys (1A)*** formed directly on the basement rocks are indicated by high Ni contents (0.12 wt %) in sulfides, which is typical for stockwork mineralization Assemblage of isocubanite, Co-pentlandite and millerite along with high Cu, Co, Ni and Se content points to high fluid temperature (>350 °C). The fluid is characterized by a range of $\delta^{34}S$ of between

+3.9‰–+4.5‰. Coincidently, Fe sulfides do not form in these chimneys. Rhythmic-layered texture of chimneys indicates a pulsing regime of fluid discharge.

Based on these characteristics, chalcopyrite chimneys mark the initial stage of "pulse-type" venting followed by stable hydrothermal discharge. Chalcopyrite chimneys are located in the centre of the discharge zone above the main fluid conduit.

2. ***Pyrrhotine-isocubanite*** chimneys are formed in two stages. During the first (2A), short-term stage, the pyrrhotite-isocubanite fine-grained aggregate is formed at high fluid temperature (350 °C). This process is also indicated by a presence of Co replacing other elements in other mineral crystal lattices (for example, Co in chalcopyrite or pyrrhotite (Table 3); the sulfide minerals precipitated from the initial portion of the fluid (δ^{34}S +3.8‰–+4.5‰).

During the second stage (2B), sulfides precipitate from fluids with temperatures lower than 350 °C and a δ^{34}S range of +6.5‰–+7.3‰. Samples with isotopically heavy δ^{34}S (+6.5‰–+7.3‰) indicate that sulfides were likely formed as a result of anhydrite replacement. Fine-fragmented aggregates of sulfides in the central part of the chimney mark dissolved anhydrite areas (Figure 5f). At these parameters sphalerite and Co-As accessory minerals also precipitate. These second stage fluids alter the first stage sulfides: pyrrhotite altered to Fe-sulfides and isocubanite altered to Y-phase (Table 3). New generations of unaltered pyrrhotite-isocubanite and Fe-sphalerite (Fe average 15.06 wt %—Table 3) are deposited in the cracks and cavities. Fe-sphalerite also forms a thin discrete outer layer and platy outgrowth on the chimney.

We propose that pyrrhotite-isocubanite chimneys mark the initial stage of the stable hydrothermal activity starting from the "stable intensity" high-temperature fluid discharge. These chimneys are located next to chalcopyrite ones in the main discharge zone and penetrate the anhydrite rim. We propose that the initial stage of "stable intensity", high temperature fluid discharge destroys the pre-existing chalcopyrite chimneys.

3. ***Sphalerite chimney*** formation and composition is quite variable and represented by two types. The first type (3A) of sphalerite chimneys are formed at high- and medium-temperature from a fluid ranging in δ^{34}S +4.1‰–+4.4‰. These varieties are located directly on the basement and are characterized by Fe-sphalerite (Fe content 16–20 wt %), wurtzite and polytype of wurtzite, rudashevskyite-2H (Fe content up to 50 wt %). The accessory minerals are represented by cobaltite and electrum. Extremely high content of Sn (up to 1800 ppm), Ge (up to 200 ppm) and Cd (up to 1700 ppm) are typical for these samples.

The second type (3B) of sphalerite chimneys are formed at medium- and low-temperature from fluids (δ^{34}S +6.5‰–+14‰) and marked by low Fe content in sphalerite (1–10 wt %), abundant galena and the presence of Ag-minerals.

Thus, the sphalerite chimneys are formed at a stable stage of hydrothermal activity and their composition is controlled by the distance from the main discharge zone. The high- and medium-temperature Zn chimneys (type 3A) are located close to the centre of the discharge zone and enriched in Fe, Sn and Ge. Medium- and low-temperature sphalerite chimneys (3B type) with variable Cu-Fe and Zn mineral ratios are formed more distal from the discharge zone. The second type of sphalerite chimneys marks the peripheral conduit characterized by circulation of medium- and low-temperature fluids. Overall, we propose the following scheme of the Ashadze-1 ore structure and formation (Figure 11):

- The initial stage (1A) of hydrothermal activity is characterized by focused pulsing venting along with precipitation of the highest temperature; layered chalcopyrite chimneys marked centre of main conduit.
- The next stage of venting (2A) is characterized by "stable intensity" discharge and formation of pyrrhotite-isocubanite chimneys. During this stage the chalcopyrite chimneys are destroyed.
- During the next stages (2B and 3A), a lower temperature portion of fluids transforms minerals and forms a new generation of pyrrhotite and isocubanite along with Fe-wurtzite and sphalerite.

Zn-sulfide chimneys enriched in Sn and Ge are formed close to the centre of the discharge zone and main conduit.

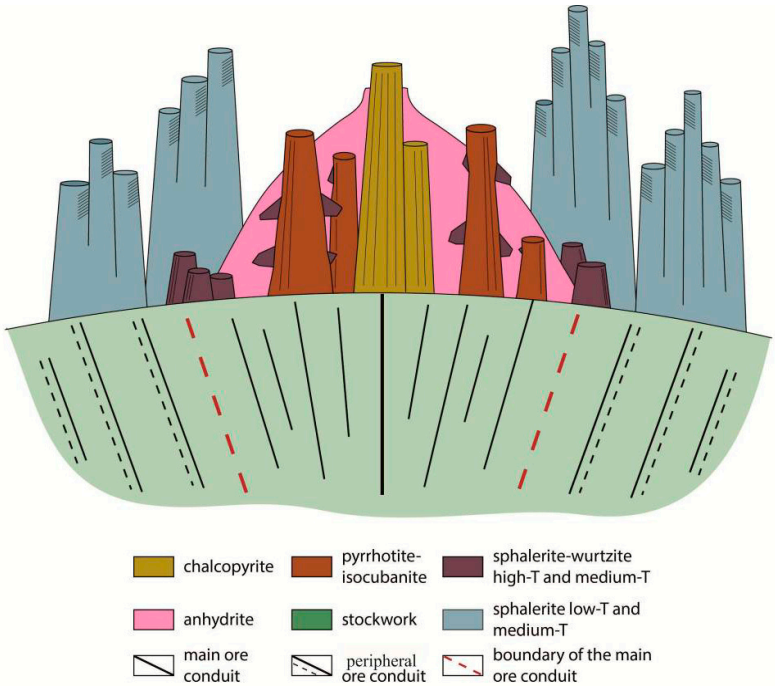

Figure 11. Scheme of ultramafic-hosted Ashadze-1 deposit structure and formation (see text for explanation).

These stages of chimney formation (1A, 2A, 2B, 3A) mark the main conduit zone at the primary stages of the sulfide ore-forming process. These chimneys were recovered from different parts of the field, exhibiting various combinations of the chimneys types. From this observation we suggest the presence of several venting centers, which migrate in space and time. This is in contradiction to other SMS sites, such as TAG, where the mound structure contains a stable location of the central venting [25]. We suggest the reason for this migration could be connected with specific properties of the host rocks. Hydrothermal alteration of ultramafic rock changes its physical properties, resulting in low density, high plasticity and permeability. These properties of the host rocks could lead to the migration of the conduit zone(s). The last stage of mineralization (3B) is connected with low-temperature low-Fe sphalerite chimneys enriched in Pb and Ag. They formed more distal to the discharge zone (Figure 11). The fluid conductively cools and mixes with seawater during the migration at the peripheral zone.

The age of the Ashadze-1 field is estimated as less than 7.1 kyr (Table 5), whereas most hydrothermal fields on the MAR are much older, up to 170 kyr [26]. The Ashadze-1 deposit is considered an example of a hydrothermal system in its initial stage of evolution marked by the young age of the sulfides (<7.2 kyr). The mineralogy of Ashadze-1 reflects primary processes, unlike other older deposits on the MAR which exhibit post formation hypergene alteration. We propose the above model as the primary ore-forming hydrothermal process in an ultramafic-hosted environment on the modern seafloor.

Acknowledgments: The authors express their thanks to Larisa Lazareva, Victor Bel'tenev, Irina Rozhdestvenskaya and Victor Ivanov for the provided samples. We would like to thank Tatiana Semkova for mineralogical data and Vladislav Kuznetsov for age determination of sulfides. The authors appreciate the valuable comments and advice from the anonymous reviewers. We are grateful to Nicholas Dyriw for reviews and editing. The study was partly financed by project 3.37.135.2014 of St. Petersburg State University.

Author Contributions: Anna Firstova wrote the paper, performed the experiments, analyzed the data. Tamara Stepanova and Georgy Cherkashov wrote the paper, analyzed the data. Alexey Goncharov performed the experiments, analyzed the data. Svetlana Babaeva analyzed the data.

Conflicts of Interest: The authors declare no conflict of interest.

Abbreviations

The following abbreviations are used in this manuscript:

MAR	Mid-Atlantic Ridge
OCC	Oceanic core complex
SMS	Seafloor massive sulfides

References

1. Rona, P.A.; Klinkhammer, G.; Nelson, T.; Trefry, J.; Elderfield, H. Black smokers, massive sulfides and vent biota at the Mid-Atlantic Ridge. *Nature* **1986**, *321*, 33–37. [CrossRef]
2. Fouquet, Y.; Cambon, P.; Etoubleau, J.; Charlou, J.; Ondréas, H.; Barriga, F.; Cherkashov, G.; Semkova, T.; Poroshina, I.; Bohn, M.; *et al*. Geodiversity of hydrothermal processes along the Mid-Atlantic Ridge and ultramafic-hosted mineralization: A new type of oceanic Cu-Zn-Co-Au volcanogenic massive sulfide deposit. In *Diversity of Hydrothermal Systems on Slow Spreading Ocean Ridges, Geophysical Monograph Series*; Rona, P., Devey, C., Dyment, J., Murton, B., Eds.; American Geophysical Union: Washington, D.C., USA, 2010; Volume 188, pp. 321–367.
3. Beaulieu, S.E.; Baker, E.T.; German, C.R.; Maffei, A. An authoritative global database for active submarine hydrothermal vent fields. *Geochem. Geophys. Geosyst.* **2013**, *14*, 4892–4905. [CrossRef]
4. Cherkashov, G.; Poroshina, I.; Stepanova, T.; Ivanov, V.; Bel'tenev, V.; Lazareva, L.; Rozhdestvenskaya, I.; Samovarov, M.; Shilov, V.; Glasby, G.; *et al*. Seafloor massive sulfides from the northern equatorial Mid-Atlantic Ridge: New discoveries and perspectives. *Mar. Georesour. Geotechnol.* **2010**, *28*, 222–239. [CrossRef]
5. Escartın, J.; Smith, D.K.; Cann, J.; Schouten, H.; Langmuir, C.H.; Escrig, S. Central role of detachment faults in accretion of slow-spreading oceanic lithosphere. *Nature* **2008**, *455*, 790–795. [CrossRef] [PubMed]
6. Bel'tenev, V.; Nescheretov, A.; Shilov, V.; Shagin, A.; Stepanova, T.; Cherkashev, G.; Batuev, M.; Samovarov, M.; Rozhdestvenskaya, I.; Andreeva, I.; *et al*. New discoveries at 12°58′ N, 44°52′ W, MAR: Professor Logatchev-22 cruise, initial results. *InterRidge News* **2003**, *12*, 13–14.
7. Cherkashov, G.; Bel'tenev, V.; Ivanov, V.; Lazareva, L.; Samovarov, M.; Shilov, V.; Stepanova, T.; Glasby, G.P.; Kuznetsov, V. Two new hydrothermal fields at the Mid-Atlantic Ridge. *Mar. Georesour. Geotechnol.* **2008**, *26*, 308–316. [CrossRef]
8. Ondreas, H.; Cannat, M.; Fouquet, Y.; Normand, A. Geological context and vents morphology of the ultramafic-hosted Ashadze hydrothermal areas (Mid-Atlantic Ridge 13° N). *Geochem. Geophys. Geosys* **2013**, *13*. [CrossRef]
9. Fouquet, Y.; Cherkashov, G.; Charlou, J.L.; Ondreas, H.; Birot, D.; Cannat, M.; Bortnikov, N.; Silantyev, S.; Sudarikov, S.; Cambon-Bonavita, M.A.; *et al*. Serpentine cruise—Ultramafic hosted hydrothermal deposits on the Mid-Atlantic Ridge: First submersible studies on Ashadze 1 and 2, Logatchev 2 and Krasnov vent fields. *InterRidge News* **2008**, *17*, 15–19.
10. Cannat, M.; Mangeney, A.; Ondreas, H.; Fouquet, Y.; Normand, A. High-resolution bathymetry reveals contrasting landslide activity shaping the walls of the Mid-Atlantic Ridge axial valley. *Geochem. Geophys. Geosyst.* **2013**, *14*, 4892–4905.
11. Mozgova, N.N.; Trubkin, N.V.; Borodaev, Y.S.; Cherkashev, G.A.; Stepanova, T.V.; Semkova, T.A.; Uspenskaya, T.Y. Mineralogy of massive sulfides from the Ashadze hydrothermal field, 13 N, Mid-Atlantic Ridge. *Can. Miner.* **2008**, *46*, 545–567. [CrossRef]
12. Lein, A.U.; Cherkashov, G.A.; Ulyanov, A.A.; Stepanova, T.V.; Sagalevich, A.M.; Bogdanov, Y.A.; Gurvich, E.G.; Torokhov, M.P. Mineralogy and geochemistry of sulfide fields Logachev-2 and Rainbow: Similarities and differences. *Geochemistry* **2003**, *3*, 304–328. (In Russian)

13. Hannington, M.D.; Jonasson, I.R.; Herzig, P.M.; Petersen, S. Physical and chemical processes of seafloor mineralization at Mid-Ocean Ridges. In *Seafloor Hydrothermal Systems: Physical, Chemical, Biological, and Geological Interaction; Monograph Series*; Humphris, S.E., Zierenberg, R.A., Mullineaux, L.S., Thomson, R.E., Eds.; American Geophysical AGU: Washington, D.C., USA, 1995; Volume 91, pp. 115–157.
14. Solomon, M.; Tornos, F.; Large, R.R.; Badham, J.N.P.; Both, R. Zn-Pb-Cu volcanic-hosted massive sulfide deposits criteria for distinguishing brine pooltype from black smoker-type sulfide deposition. *Ore Geol. Rev.* **2004**, *25*, 259–283. [CrossRef]
15. Charlou, J.; Donval, J.; Konn, C.; Ondreas, H.; Fouquet, Y. High production and fluxes of H_2 and CH_4 and evidence of abiotic hydrocarbon synthesis by serpentinization in ultramafic-hosted hydrothermal systems on the Mid-Atlantic Ridge. In *Diversity of Hydrothermal Systems on Slow Spreading Ocean Ridges, Geophysical Monograph Series*; Rona, P., Devey, C., Dyment, J., Murton, B., Eds.; American Geophysical Union: Washington, D.C., USA, 2010; Volume 188, pp. 265–296.
16. Silant'ev, S.A.; Mironenko, M.V.; Novoselov, A.A. Hydrothermal systems in peridotite substrate in slow-spreading ridge. Modeling of phase transformation and substance balance: Ascending branch. *Petrology* **2009**, *17*, 563–577. (In Russian)
17. Silant'ev, S.A.; Mironenko, M.V.; Novoselov, A.A. Serpentinite hosted hydrothermal systems of Mid-Ocean Ridges: Kinetic and thermodynamic modeling of downwelling limb of a hydrothermal circulation cell. *Geochim. Cosmochim. Acta Suppl.* **2009**, *73*, 1222.
18. Sakai, H.; Desmarais, D.J.; Ueda, A.; Moore, J.G. Concentrations and isotope ratios of carbon, nitrogen, and sulfur in ocean-floor basalts. *Geochim. Cosmochim. Acta* **1984**, *48*, 2433–2441. [CrossRef]
19. Styrt, M.; Brackman, A.J.; Holland, H.D.; Clark, B.C.; Pisutharnond, V.; Eldridge, C.S.; Ohmoto, H. The mineralogy and the isotopic composition of sulfur in hydrothermal sulfide/sulfate deposits on the East Pacific Rise, 21° N latitude. *Earth Planet. Sci. Lett.* **1981**, *53*, 382–390. [CrossRef]
20. Bogdanov, Y.; Bortnikov, N.; Vikent'ev, I. Mineralogical and geochemical features of Rainbow hydrothermal deposits and fluid related to serpentinites, Mid-Atlantic Ridge (36°14′ N). *Geol. Ore Depos.* **2002**, *44*, 510–542. (In Russian)
21. Shanks, W.C. Stable isotopes in seafloor hydrothermal systems: Vent fluids, hydrothermal deposits, hydrothermal alteration, and microbial processes. *Rev. Miner. Geochem.* **2001**, *43*, 469–525. [CrossRef]
22. Shanks, W.C., III; Seyfried, W.E., Jr. Stable isotope studies of vent fluids and chimney minerals. Southern Juan de Fuca Ridge: Sodium metasomatism and seawater sulfate reduction. *J. Geophys. Res.* **1987**, *92*, 11387–11399. [CrossRef]
23. Woodruff, L.G.; Shanks, W.C., III. Sulfur isotope studies of chimney minerals and vent fluids from 21° N, East Pacific rise: Hydrothermal sulfur sources and disequilibrium sulfate reduction. *J. Geophys. Res.* **1988**, *93*, 4562–4572. [CrossRef]
24. Janecky, D.R.; Shanks, W.C., III. Computational modelling of chemical and sulfur isotopic reaction processes in seafloor hydrothermal systems: Chimneys. Massive sulfides and subjacent alteration zones. *Can. Miner.* **1988**, *26*, 603–625.
25. Hannington, M.D.; Galley, A.G.; Herzig, P.M.; Petersen, S. Comparison of the TAG mound and stockwork complex with cyprus-type massive sulfide deposits. *Proc. Ocean Drill. Program Sci. Results* **1998**, *158*, 389–414.
26. Kuznetsov, V.; Tabuns, E.; Kuksa, K.; Cherkashov, G.; Maksimov, F.; Zherebtsov, I.; Grigoriev, V.; Baranova, N.; Bel'Tenev, V.; Lazareva, L. The oldest seafloor massive sulfide deposits at the Mid-Atlantic Ridge: ^{230}Th/U chronology and composition. *Geochronometria* **2005**, *42*, 100–106. [CrossRef]